Di-electron Widths of the Upsilon(1S,2S,3S) Resonances

J. Pivarski,[1] J.R. Patterson,[1] and K. Berkelman[1]
(CLEO Collaboration)
[1]*F. R. Newman Laboratory for Elementary-Particle Physics, Ithaca, New York 14853-8001*
(Dated: November 17, 2005)

We have determined the widths for decay to e^+e^- (di-electric width, or Γ_{ee}) of $\Upsilon(1S)$, $\Upsilon(2S)$, and $\Upsilon(3S)$ to high precision from the production cross-section of each resonance, integrated over e^+e^- energies. These integrals were performed by fitting resonance lineshapes, scanned in beam energy by the Cornell Electron Storage Ring. We select hadronic Υ decays and quantify backgrounds with a large continuum sample just below each resonance. The product of di-electric widths and hadronic branching fractions, or $\Gamma_{ee}\Gamma_{\rm had}/\Gamma_{\rm tot}$, are (1.252 ± 0.005 *(stat)* ± 0.019 *(syst)*) keV, (0.581 ± 0.006 ± 0.009) keV, and (0.413 ± 0.004 ± 0.006) keV, respectively, and the di-electric widths are (1.354 ± 0.005 ± 0.020) keV, (0.619 ± 0.007 ± 0.009) keV, and (0.446 ± 0.004 ± 0.007) keV. We also report ratios of widths, (in which some systematic uncertainties cancel.

PACS numbers: What's this PACS thing?

Since the discovery of the Υ mesons ($b\bar{b}$) decades ago [1], their widths for decay to e^+e^- have been related to the quark-antiquark spatial wave function at the origin [2]. More recently, the widths have been recognized as a testing ground for the validity of approximations in QCD lattice gauge theory calculations [3]. Improvements in the lattice calculations, such as the avoidance of the quenched approximation [4], provide an incentive for more accurate experimental tests. Prior to the experiment reported here, the Γ_{ee} of the $\Upsilon(1S)$, $\Upsilon(2S)$, and $\Upsilon(3S)$ have been known to 2.2%, 4.2%, and 9.4% [5]. If the lattice calculations can be validated at the 2% level, similar calculations can provide more reliable QCD results needed for the extraction of important weak interaction parameters from experimental data. Examples include the $D_{(s)}$ and $B_{(s)}$ meson decay constants $f_{D_{(s)}}$ and $f_{B_{(s)}}$ used in the determination of the CKM parameter V_{td} (V_{td}/V_{ts}).

Our measurement of Γ_{ee} follows the method of [5]: we measure the production cross-section of the time-reversed process, $e^+e^- \to \Upsilon$, integrated over incident e^+e^- energies. Then,

$$\Gamma_{ee} = \frac{{M_\Upsilon}^2}{6\pi^2} \int \sigma(e^+e^- \to \Upsilon)\, dE, \qquad (1)$$

ignoring radiative effects. Since the measurement of decay rate is independent of the branching fraction $\mathcal{B}_{ee}$, we use $\Gamma = \Gamma_{ee}/\mathcal{B}_{ee}$ to determine the Υ full width, assuming $\mathcal{B}_{ee} = \mathcal{B}_{\mu\mu}$ to take advantage of the best-measured leptonic branching fraction [6].

To measure Γ_{ee}, the Cornell Electron Storage Ring (CESR), a symmetric e^+e^- collider, scanned center-of-mass energies in the vicinity of the $\Upsilon(1S)$, $\Upsilon(2S)$, and $\Upsilon(3S)$ and the CLEO-III detector collected the Υ decay products to determine the cross-section at each energy. The integral in Equation 1 is then extracted by a fit to this resonance lineshape. The fit includes beam energy spread, initial state radiation, backgrounds, and interference between Υ and continuum final states. The $\Upsilon(1S)$, $\Upsilon(2S)$, and $\Upsilon(3S)$ scans have an integrated luminosity of 0.27, 0.08, and 0.22 fb^{-1} each, with 0.19, 0.41, and 0.14 fb^{-1} of continuum data 20 MeV below each peak energy to constrain backgrounds.

The CLEO-III detector is a nearly 4π tracking volume surrounded by a CsI crystal calorimeter [7]. Charged tracks are reconstructed in a 47-layer wire drift chamber and 4-layer silicon strip detector, and their momenta are inferred from their radii of curvature in a 1.5 T magnetic field. The calorimeter forms a cylindrical barrel around the tracking volume, reaching angles θ with respect to the beam axis of $|\cos\theta| < 0.85$, with endcaps extending this range to $|\cos\theta| < 0.98$. Electron showers have a resolution of x MeV at beam energy (5 GeV).

The Υ mesons are produced nearly at rest and decay into leptonic final states e^+e^-, $\mu^+\mu^-$, and $\tau^+\tau^-$, or into hadrons with a typical multiplicity of ten through strong decay via ggg and $gg\gamma$, or through electromagnetic decay via a virtual photon and $q\bar{q}$ states. The $\Upsilon(2S)$ and $\Upsilon(3S)$ can also make transitions into other $b\bar{b}$ resonances such as $\chi_{bJ}(nP)$, $\Upsilon(1S)$, and $\Upsilon(2S)$. The leptonic decays together account for only about 7% of the decays of each resonance and are difficult to distinguish from background, so we select hadrons, fit the hadronic cross-section, and report $\Gamma_{ee}\Gamma_{\rm had}/\Gamma_{\rm tot}$. We then correct for the missing leptonic modes to report Γ_{ee}.

Bhabha scattering ($e^+e^- \to e^+e^-$) is our largest background. We suppress these events by requiring the greatest track momentum to be less than 80% of the beam energy, shown in Figure 1-a, which reduces the Bhabha background to approximately the same magnitude as the hadronic continuum ($e^+e^- \to q\bar{q}$) background. Continuum annihilation processes such as these are all accounted for by including a $1/s$ term in the lineshape fit.

Two-photon fusion events ($e^+e^- \to e^+e^-X$) contribute a non-$1/s$ background, so we suppress these by requiring the total visible energy (energy sum of all charged

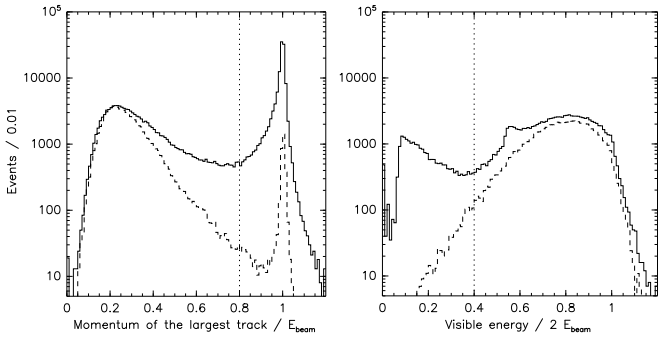

FIG. 1: Two of the four hadronic selection criteria: (a) the greatest track momentum must be less than 80% of the beam energy, and (b) the visible energy in the event must be more than 40% of the center-of-mass energy. Solid histograms are data, dashed are simulated Υ decays. All hadronic selection criteria are applied except the one shown. Note the log scale.

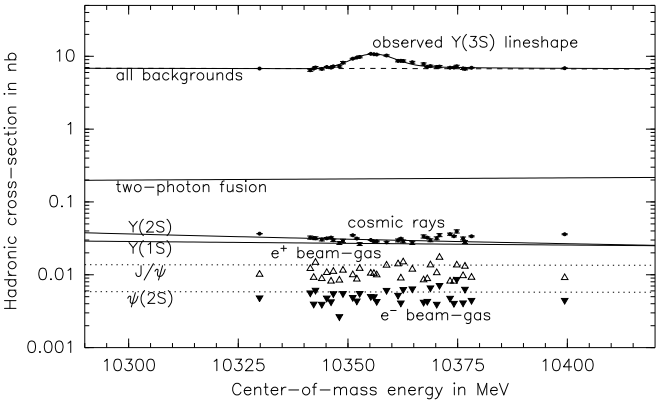

FIG. 2: Selected events divided by luminosity in log scale, to show background components. The top curve, fitted to data, is the hadron count and the dashed line below it represents all continuum and $\tau^+\tau^-$ backgrounds. The three curves far below that are non-$1/s$ corrections to the continuum, and the three sets of points (not related to the curves) are cosmic ray and beam-gas estimations for each energy run, which have been explicitly subtracted from the hadron count.

tracks and neutral showers) to be more than 40% of the center-of-mass energy (twice the beam energy), shown in Figure 1-b. A small $\log s$ term (8% of continuum below $\Upsilon(1S)$) and a $1/(\sqrt{s} - M_\Upsilon)$ term representing radiative returns to each of the lighter Υ resonances (about 0.5% of continuum) are also added to the fit function. Because the continuum measurement is only 20 MeV below the resonance, the different functional forms affect the background estimation at the peak by less than 0.04%.

Cosmic rays and beam-gas (collisions between a beam electron and a gas nucleus inside the beampipe) are suppressed by requiring charged tracks to point toward the collision point. We reduce this to 1% of the continuum by demanding that at least one reconstructed track pass within 5 mm of the beam axis and the vertex reconstructed from all primary tracks be within 7.5 cm of the collision point along the beam axis. We determine the contamination at each energy using special single-beam and no-beam data runs normalized using events with a solitary large impact parameter track (for cosmic rays) or events with vertices along the beam axis but far from the collision point (for beam gas).

Backgrounds are summarized in Figure 2.

While our hadronic selection criteria eliminate essentially all $\Upsilon \to e^+e^-$ and $\Upsilon \to \mu^+\mu^-$ decays, they accept 57% of $\Upsilon \to \tau^+\tau^-$, according to a GEANT-based Monte Carlo simulation [8] including final state radiation [9]. We therefore include in the fit function an $\Upsilon \to \tau^+\tau^-$ background term using the measured $\mathcal{B}_{\tau\tau}$ [10].

A small fraction of hadronic Υ decays fail our event selection criteria, so we correct for this inefficiency. Instead of estimating it with the Monte Carlo simulation, which would introduce dependence on the hadronization and decay models and the detector simulation, we use a data-based approach. We select $\Upsilon(2S) \to \pi^+\pi^-\,\Upsilon(1S)$ to study $\Upsilon(1S)$ decays tagged by the $\pi^+\pi^-$. If the $\pi^+\pi^-$ were sufficient to satisfy the trigger, the efficiency would be the ratio of $\Upsilon(1S)$ events satisfying our selection criteria (excluding the $\pi^+\pi^-$ tracks and calorimeter signals) to all $\Upsilon(1S)$ events.

We can apply the above procedure directly using a 1.3 fb^{-1} sample at the $\Upsilon(2S)$ peak and a special two-track trigger, but this trigger is prescaled, so this procedure can only determine the hadronic efficiency to 3% of itself. Therefore, we use the two-track trigger to determine the efficiency of an unprescaled but more restrictive hadronic trigger ($\epsilon_{\rm htrig}$), and then use the full statistics from the hadronic trigger to determine our selection efficiency, once this trigger has been satisfied ($\epsilon_{\rm cuts}$). Our selection efficiency is then the product of $\epsilon_{\rm htrig}$ and $\epsilon_{\rm cuts}$.

The mass of the system recoiling against the $\pi^+\pi^-$ candidates in the two-track trigger sample is shown in Figure 3-a and the subset of events that fail the hadronic trigger is shown in Figure 3-b. After correcting for leptonic decays in the $\Upsilon(1S)$ sample, we find $\epsilon_{\rm htrig} = (99.59\ ^{+0.29}_{-0.45})\%$ from the ratio of fit yields.

Using $\Upsilon(2S) \to \pi^+\pi^-\,\Upsilon(1S)$ events that satisfy the hadronic trigger, we find $\epsilon_{\rm cuts} = (98.46 \pm 0.30)\%$. This has been corrected for leptonic decays, the boost of the $\Upsilon(1S)$, track and shower confusion from the $\pi^+\pi^-$, and bias in trigger efficiency from the $\pi^+\pi^-$. Only the first correction is significant. Our event selection efficiency is therefore $(97.93\ ^{+0.44}_{-0.56})\%$ for the sum of all Υ decays other than e^+e^-, $\mu^+\mu^-$, and $\tau^+\tau^-$.

To find the $\Upsilon(2S)$ and $\Upsilon(3S)$ efficiencies, we correct the $\Upsilon(1S)$ efficiency for energy dependence and for transitions specific to these excited states, using simulations. Energy dependence in ggg, $gg\gamma$, $q\bar{q}$, and the presence of most transitions have little effect on the $\Upsilon(2S)$ and $\Upsilon(3S)$ efficiencies (a 0.2% downward correction), but transitions

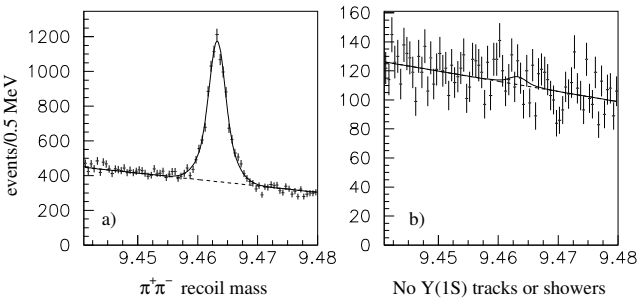

FIG. 3: Mass of the system recoiling against $\pi^+\pi^-$ candidates in the hadronic efficiency study, (a) for all events from the two-track trigger and (b) for those which fail the hadronic trigger. The solid line is a double Gaussian fit with a linear background (dashed). In (b), the mean, sigmas, and area ratio of the double Gaussian are not allowed to float.

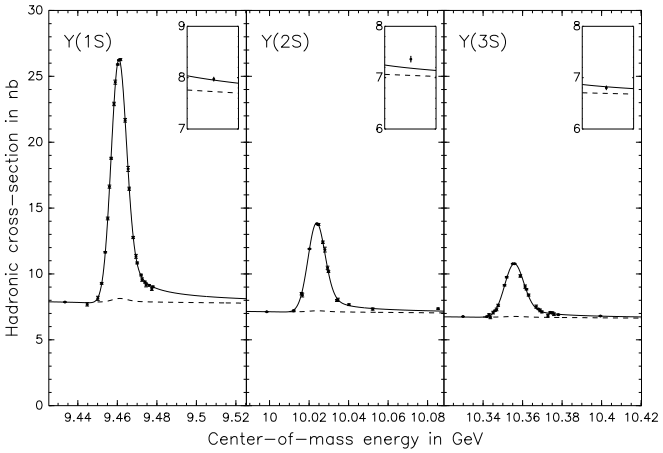

FIG. 4: Fits to $\Upsilon(1S)$, $\Upsilon(2S)$, and $\Upsilon(3S)$ hadronic cross-section versus center-of-mass energy lineshapes, left to right. Points are data, corrected for fitted beam energy shifts between scans, the solid line is the fit, the dashed line is sum of all backgrounds, and the insets show high-energy measurements. The continuum background is not purely hadronic.

to a lower Υ which then decay to e^+e^- or $\mu^+\mu^-$ usually fail our event selection. We measure the branching fractions of these $X\ell^+\ell^-$ decays to be $(1.58 \pm 0.16)\%$ and $(1.34 \pm 0.13)\%$, respectively, resulting in $\Upsilon(2S)$ and $\Upsilon(3S)$ efficiencies of $(96.18\ ^{+0.44}_{-0.56} \pm 0.15)\%$ and $(96.41\ ^{+0.44}_{-0.56} \pm 0.13)\%$, where the first uncertainty is common to all three resonances.

We use Bhabha events to determine the relative luminosity of each scan point. We select the Bhabhas by requiring two or more central tracks with measured momenta between 50% and 110% of the beam energy, and E/p consistent with e^+e^-. Contamination from $\Upsilon \to e^+e^-$ is 2–5% and is readily calculated given $\mathcal{B}_{\mu\mu}$ once we have done our Υ lineshape fit. Our subtraction includes energy-dependent interference between $\Upsilon \to e^+e^-$ and Bhabhas.

We determine the overall luminosity scale using the method of [11] from Bhabhas, $e^+e^- \to \mu^+\mu^-$, and $e^+e^- \to \gamma\gamma$, with the Babayaga event generator [12]. The systematic uncertainties in the luminosity for the three final states are 1.6%, 1.6%, and 1.8%, respectively, dominated by track finding and resonance interference for the leptonic final states, and by photon finding and cut variation for $\gamma\gamma$. The three final states give consistent results off-resonance, where Υ contamination is negligible. We use the weighted mean to determine the luminosity, and take the RMS scatter of 1.3% as the systematic uncertainty.

Bhabha and $\gamma\gamma$ luminosity, normalized to the same value off-resonance, deviate by $(0.8 \pm 0.2)\%$, $(0.3 \pm 0.4)\%$, and $(0.7 \pm 0.2)\%$ when extrapolated to the $\Upsilon(1S)$, $\Upsilon(2S)$, and $\Upsilon(3S)$ peaks. We correct Γ_{ee} downward by half of this discrepancy and add half the discrepancy and its uncertainty in quadrature to the systematic uncertainty of each resonance.

Accurate measurements beam energy differences are also important for determining Γ_{ee}. The beam energy is measured by an NMR probe in a test dipole magnet in series with the beam magnets, with corrections for RF frequency shifts, steering and focusing magnets, and electrostatic electron-positron separators. To limit our sensitivity to drifts in this measurement, we limit scans to 48 hours and alternate measurements above and below the peak. While repeated scans indicate that the calibration of the ∼5 GeV beam energy drifts as much as 0.3 MeV between scans, repeated resonance cross-section measurements at the same energy during a scan indicate that the beam energy calibration drifts by less than 0.04 MeV within a scan (68% C.L.), which translates to a 0.2% uncertainty in Γ_{ee}.

The data for the energy scan of each of the three resonances are independently fit to a lineshape function that consists of a three-fold convolution of (a) a Breit-Wigner resonance function including interference between the electromagnetic $q\bar{q}$ portion of the resonance decays with the continuum $q\bar{q}$ cross-section, (b) an initial state radiation distribution as given in Equation 28 of Kuraev and Fadin [13], and (c) the Gaussian spread in CESR beam energy, plus the background terms described above. The radiative corrections account for emission of real and virtual photons by the initial e^+e^-. It does not correct for vacuum polarization, which is thereby absorbed into the definition of Γ_{ee}. The resulting Γ_{ee} values therefore should represent the Born diagram coupling a pure e^+e^- state to the Υ. The lineshape fits are insensitive to the Breit-Wigner widths, which are fixed to the PDG values. The value of $\Gamma_{ee}\Gamma_{\rm had}/\Gamma_{\rm tot}$ is allowed to float, as well as the continuum normalization, and, to remove sensitivity to beam energy shifts between scans, the peak energy of each scan. In addition, we fit for the beam energy spread of groups of scans with common CESR

Contribution to Γ_{ee}	$\Upsilon(1S)$	$\Upsilon(2S)$	$\Upsilon(3S)$
Scaled statistical uncertainty	1.3×0.3%	1.6×0.7%	1.0%
$(1-3\mathcal{B}_{\mu\mu})$	0.2%	0.2%	0.3%
Hadronic efficiency	⟵	0.5%	⟶
Xe^+e^-, $X\mu^+\mu^-$ correction	0	0.15%	0.13%
Overall luminosity scale	⟵	1.3%	⟶
Bhabha/$\gamma\gamma$ inconsistency	0.4%	0.4%	0.4%
Beam energy measurement drift	0.2%	0.2%	0.2%
Shape of the fit function	0.1%	0.1%	0.1%
Total (summed in quadrature)	1.5%	1.9%	1.8%

TABLE I: All uncertainties in Γ_{ee} measurements in the order in which they are discussed in the text (except statistical uncertainty, which is presented first). Uncertainties that are common to all resonances are indicated with arrows.

$\Gamma_{ee}\Gamma_{\rm had}/\Gamma_{\rm tot}(1S)$	$(1.252 \pm 0.005 \pm 0.019)$ keV
$\Gamma_{ee}\Gamma_{\rm had}/\Gamma_{\rm tot}(2S)$	$(0.581 \pm 0.006 \pm 0.009)$ keV
$\Gamma_{ee}\Gamma_{\rm had}/\Gamma_{\rm tot}(3S)$	$(0.413 \pm 0.004 \pm 0.006)$ keV
$\Gamma_{ee}(1S)$	$(1.354 \pm 0.005 \pm 0.020)$ keV
$\Gamma_{ee}(2S)$	$(0.619 \pm 0.007 \pm 0.009)$ keV
$\Gamma_{ee}(3S)$	$(0.446 \pm 0.004 \pm 0.007)$ keV
$\Gamma_{ee}(2S)/\Gamma_{ee}(1S)$	$(0.457 \pm 0.006 \pm 0.003)$
$\Gamma_{ee}(3S)/\Gamma_{ee}(1S)$	$(0.329 \pm 0.004 \pm 0.002)$
$\Gamma_{ee}(3S)/\Gamma_{ee}(2S)$	$(0.720 \pm 0.011 \pm 0.006)$

TABLE II: The results of $\Gamma_{ee}\Gamma_{\rm had}/\Gamma_{\rm tot}$ for the three resonances, the di-electron widths Γ_{ee}, and their ratios. The first uncertainty is scaled statistical and the second is systematic (everything else).

horizontal steerings, but allow shifts when the steerings change, since they can change the beam energy spread by 1%. The largest systematic uncertainties in the shape of the fit function come from the radiative corrections and $\tau^+\tau^-$ normalization: these lead to a 0.1% uncertainty in $\Gamma_{ee}\Gamma_{\rm had}/\Gamma_{\rm tot}$.

The fit results are plotted in Figure 4. The reduced $\chi^2 = \chi^2/(N_{\rm pt} - N_{\rm dof})$ for $\Upsilon(1S)$, $\Upsilon(2S)$, and $\Upsilon(3S)$ are $240/(203-16) = 1.3$, $107.2/(75-9) = 1.6$, and $155/(175-16) = 0.97$, respectively. Pull distributions versus energy and versus date show no obvious trends. Therefore, we take the large reduced χ^2 values as an indication that uncorrelated uncertainties are underestimated, and increase the statistical uncertainty accordingly.

All uncertainties are listed in Table I.

Our values of $\Gamma_{ee}\Gamma_{\rm had}/\Gamma_{\rm tot}$, listed in Table II, are consistent with, but more precise than, but PDG world averages [5] and provide the first precise measurement of the $\Upsilon(3S)$. We assume $\mathcal{B}_{ee} = \mathcal{B}_{\mu\mu} = \mathcal{B}_{\tau\tau}$ and obtain $\mathcal{B}_{\mu\mu}$ from [6] to determine Γ_{ee} and ratios of Γ_{ee} for the three resonances, also listed in the Table. Dividing Γ_{ee} by $\mathcal{B}_{\mu\mu}$, we obtain new values of the Υ full widths: 54.4 ± 1.8 keV, 30.5 ± 1.4 keV, and 18.6 ± 1.0 keV, respectively.

We gratefully acknowledge the effort of the CESR staff in providing us with excellent luminosity and running conditions. This work was supported by the A.P. Sloan Foundation, the National Science Foundation, and the U.S. Department of Energy.

[1] I'm not really sure
[2] what Karl
[3] had in mind...
[4] A. Gray, I. Allison, C. T. H. Davies, E. Gulez, G. P. Lepage, J. Shigemitsu and M. Wingate, arXiv:hep-lat/0507013.
[5] S. Eidelman *et al.* [Particle Data Group], Phys. Lett. B **592**, 1 (2004).
[6] G. S. Adams *et al.* [CLEO Collaboration], Phys. Rev. Lett. **94**, 012001 (2005).
[7] G. Viehhauser *CLEO III Operation*, Nucl. Instrum. Methods A **462**, 146 (2001).
[8] R. Brun *et al.*, Geant 3.21, CERN Program Library Long Writeup W5013 (1993), unpublished.
[9] E. Barberio and Z. Wąs, Comput. Phys. Commun. **79**, 291 (1994).
[10] $\mathcal{B}_{\tau\tau}$: conference proceeding?
[11] G.D. Crawford *et al.* (CLEO Collaboration), Nucl. Instrum. Methods Phys. Res., Sect A **345**, 429 (1994).
[12] C.M. Carloni Calame *et al.*, Nucl. Phys. Proc. Suppl. B **131**, 48 (2004).
[13] E. A. Kuraev and V. S. Fadin, Sov. J. Nucl. Phys. **41**, 466 (1985) [Yad. Fiz. **41**, 733 (1985)].